INORGANIC CHEMISTRY
FRONTIERS

REVIEW

View Article Online
View Journal | View Issue

Cite this: *Inorg. Chem. Front.*, 2020, **7**, 4939

Application of MOF-derived transition metal oxides and composites as anodes for lithium-ion batteries

Xiaohong Tan, †[a] Yongbo Wu,†[b] Xiaoming Lin, *[a] Akif Zeb, [a] Xuan Xu,*[a] Yifan Luo[a] and Jincheng Liu*[c]

Metal–organic frameworks (MOFs) have potential application prospects in the electrochemical energy storage and conversion area on account of their high specific surface area, high porosity, tunable pore size, and structural diversity when compared to traditional porous materials. In order to expand the application scope of MOFs, thermal decomposition can be carried out *via* calcination treatment in order to convert them into porous metal oxide materials. In this review, we summarize the synthetic methods of MOF-derived transition metal oxide (TMO) composites and their applications in lithium-ion batteries (LIBs) as anodes. A variety of TMOs and composites with different structures and morphologies derived from MOFs based on several types of ligands, including 1,4-benzenedicarboxylic acid (H_2BDC), 1,3,5-benzenetricarboxylic acid (H_3BTC), 2-methylimidazole, ferricyanide, and other unusual organic linkers, have been discussed. Finally, current challenges and possible solutions of MOF-derived anode materials have been proposed.

Received 3rd August 2020,
Accepted 7th October 2020

DOI: 10.1039/d0qi00929f

rsc.li/frontiers-inorganic

1. Introduction

Environmental and energy issues are two of the most serious problems of the 21st century. The key to solving these problems is to produce renewable energy in a green and environmentally friendly way. In order to maximize the utilization rate of electrical energy and minimize environmental pollution, much effort has been put into the design and advancement of efficient electrochemical energy storage and conversion technology. Lithium ion batteries (LIBs) are considered to be one of the significant breakthroughs in the electrochemical energy storage area in the recent decades.[1,2] The practical applications of LIBs include electric and hybrid vehicles, portable electronic devices and smart grids due to their advantages of low cost, long cycle performance, small size, high energy density, high reversible capacity, and no memory effect.[3,4] Until now, graphite has been considered as a commercial material for Li-ion battery anodes. However, the traditional graphite anode has problems of relatively low theoretical capacity (372 mA h g^{-1}) and low efficiency, which are insufficient to fulfill the growing demand of energy storage.[5] Therefore, development and fabrication of new anode materials with excellent electrochemical behavior are the need of the hour.

Metal–organic frameworks (MOFs), as a new category of porous crystal nanomaterials composed of metal centers and organic linkers, have been applied in a wide range of applications, such as gas storage and separation,[6] catalysis,[7] drug delivery,[8] and energy storage and conversion,[9–11] owing to their tunable pore size, high specific surface area, and distinct morphology. It is well known that the structures of electrode materials have a significant effect on the electrochemical properties of batteries. One of the first MOFs that was used as an anode material for LIBs was MOF-177.[12] Unfortunately, MOFs are not suitable for direct use as electrode materials for LIBs due to the disadvantage of poor electronic conductivity. However, they have been widely used as potential precursors and templates in order to fabricate transition metal oxides (TMOs) for LIBs by taking advantage of their designable and unique advantages: (1) self-template-directed formation of metal oxides with controllable particle size, shape and morphology can be achieved *via* calcinations of MOFs. In particular, the nano-size and hollow/porous structure can offer more active sites, shortening the distance of ion transport and buffering the volume expansion. (2) Multimetallic oxides can be readily prepared from heterometallic MOFs as precursors under calcina-

[a]*School of Chemistry, South China Normal University, Guangzhou, 510006, P. R. China. E-mail: linxm@scnu.edu.cn, xuxuan@scnu.edu.cn*
[b]*School of Physics and Telecom Engineering, South China Normal University, Guangzhou, 510006, P. R. China*
[c]*EVE Energy Company Limited, Huizhou, Guangdong 516006, P. R. China. E-mail: ljc@evebattery.com*
†These authors contributed equally to this work.

tions, and they deliver better electrochemical performance when compared to their counterpart single metal oxides due to the synergistic effect between metal species. (3) MOFs are considered as a rich source of carbon and nitrogen, and the *in situ* resulting carbon and nitrogen atoms can be retained at proper temperature and atmosphere, which can enhance the electrochemical performance and mechanical stability of the final materials in the anode application. Meanwhile, another effective approach has been adopted by mixing excellent conductive materials such as carbon cloth, carbon nanotubes and carbon fiber as flexible and sturdy substrates to obtain TMO/carbon hybrids as competent anode materials for LIBs.

The electrochemical application of MOFs and their derivatives have made considerable advancements in the past several years, and reviews have summarized the previous investigations of MOFs for electrochemical energy storage applications.[13–15] Compared with other MOF derivatives, transition metal oxides have attracted most attention and present more superiority, probably due to their high capacities and ease of handling. MOFs precursors can convert into corresponding TMOs through one or two-step thermal treatment. However, post-acid washing treatment is necessary to completely remove the residual metallic species within the MOF-derived carbon matrix. However, for MOF-derived nitrides and phosphides, the comparable large volume expansion is approximately twice as high compared to that of TMOs, potentially causing obvious mechanical deterioration of the electrode during cell reaction.[16,17] The sulfides derived from MOFs usually involve in complicated preparation processes, and the products are also harmful and toxic. In the following, the application prospects of MOF-derived metal oxides for Li-ion batteries have been discussed (Fig. 1). The synthetic strategies, composition, morphology, and structure–performance relationship are briefly introduced. Finally, the problems and challenges of MOF-derived TMOs as anode materials for LIBs are highlighted, and some possible solutions and prospects for future applications are also proposed.

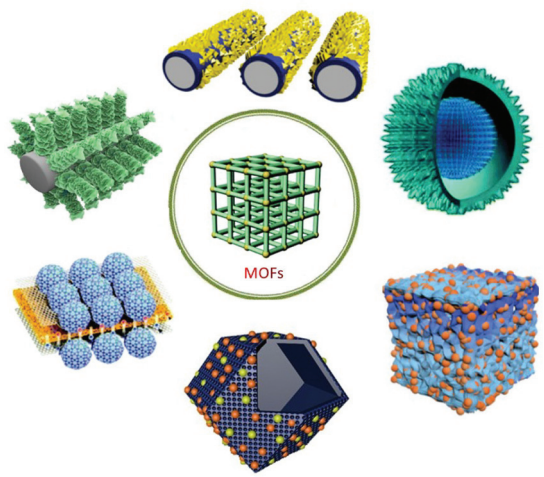

Fig. 1 MOFs and MOF–derived metal oxides.[65–70]

2. MOF-derived TMOs and composites as anode materials for LIBs

MOFs are sometimes also named porous coordination polymers (PCP). The abbreviation "MOFs" was popularized by O. M. Yaghi, the pioneer who devoted considerable efforts to the assembly of extended frameworks and molecular level-controlled orientation in solid-state building blocks containing transition metal cations and organic linkers.[71,72] The term "MOF" was used since such materials can be fully activated to show permanent porosity by removing the solvent molecules in the pore. The immense possibilities of linking inorganic metal ions and organic ligands created a breakthrough, which resulted in the synthesis of a huge number of MOFs and further studies of their applications in various research areas, including energy storage and conversion. However, without any pretreatment, pristine MOFs often face problems when used as anode materials for LIBs, which include poor conductivity, short cycling life, and incomplete electrode reaction. Fortunately, enormous porous TMOs based on an MOF-template have been obtained through facile pyrolysis in inert gas or in air. MOF-derived TMOs and their composites have lots of advantages, such as controllable chemical composition, adjustable porosity, high surface area, and shortened ion and electron transmission distance. Although great progress has been achieved in the synthesis of MOF-derived TMOs for the application of anodes in LIBs, they are mainly concentrated on different MOFs based on 1,4-benzenedicarboxylic acid (H_2BDC), 1,3,5-benzenetricarboxylic acid (H_3BTC), 2-methylimidazole, and ferricyanide, probably due to their low cost and strong coordination ability. The superiority of these organic linkers resulted in the gathering of a series of representative MOFs, such as ZIF-67, ZIF-8, MOF-5, and HKUST-1, with the possibility of large-scale production with easy modifications, and they are even easily available from commercial sources. Therefore, we focused on these organic linker based MOFs to provide a particular classification and full-scale discussion to show the merits of these organic linkers over other organic linkers in the preparation of TMOs and their composites. Table 1 lists the precursors, preparation and LIB anodic performance of these MOF-derived TMOs and composites.

2.1. TMOs derived from 1,4-benzenedicarboxylic acid based MOFs

One of the typical representatives of the MOF series of organic framework compounds is MOF-5. As a three-dimensional porous structure material, MOF-5 is composed of an organic linker (1,4-benzenedicarboxylate) and a metal center (Zn^{2+}). The inorganic $[OZn_4]^{6+}$ groups are connected to an octahedral array of $[O_2C–C_6H_4–CO_2]^{2-}$ groups, where an oxygen-centered Zn_4 tetrahedron ($[OZn_4(CO_2)_6]$) occupies each corner that is linked by six carboxylates of organic linkers.[73] Due to the strong coordination ability and low cost, many analogues of this MOF have been prepared by using different metal ions (Zn^{2+}, Co^{2+}, Cu^{2+}, Mg^{2+}, Ni^{2+}, and Al^{3+}) and same type ligands.

Table 1 Various transition metal oxides and composites derived from different ligand based MOFs as anode materials for LIBs

Precursor	Synthesis method	Target product	Current density ($mA\ g^{-1}$)	Cycle number	Reversible capacity ($mA\ h\ g^{-1}$)	Ref.
Ni-BDC	Heated at 250–300 °C	Nanoparticles NiO	1000	100	410	18
Sn-BDC	Thermal treatment in air for 2 h at 400 °C (5 °C min^{-1})	Nanoparticles SnO_2	400	100	541	19
MIL-125(Ti)	Calcination under air for 5 h at 380 °C (10 °C min^{-1})	Porous TiO_2	168	500	166	20
MIL-125(Ti)	Calcination under air atmosphere	Hierarchical porous TiO_2	840	200	155	21
Fe-BDC	Pyrolysing for 2 h at 550 °C (5 °C min^{-1})	Spindles α-Fe_2O_3	100	40	921	22
MIL-53(Fe)	Annealing in air for 30 min at 500 °C (5 °C min^{-1})	Yolk–shell Fe_2O_3	100	200	1176	23
CoBDC	Calcination for 5 h at 500 °C	Nanosheets Co_3O_4	1000	200	775	24
[Co(bdc)(DMF)]	Calcination in air for 12 h at 300 °C (10 °C min^{-1})	Mesoporous Co_3O_4	200	60	913	25
Co–V-BDC	Heated in air for 4 h at 450 °C	Sponge $Co_3V_2O_8$	1000	700	501	26
Co–V-BDC	Heated at 250–300 °C	Microsphere $Co_3V_2O_8$	5000	400	650	27
Zn–Co-BDC	Annealing in air for 2 h at 500 °C (5 °C min^{-1})	Nanosheets ZnO/$ZnCo_2O_4$	2000	250	1016	28
Zn–Ni-BDC	Calcination for 20 min at 450 °C (2 °C min^{-1})	Yolk–shell ZnO/NiO	500	1000	592	29
Fe(III)-MOF-5	Heated in N_2 at 500 °C (1 °C min^{-1})	Octahedra ZnO/$ZnFe_2O_4$/C	2000	100	988	30
Zn/Fe-BDC	Calcination in N_2 for 2 h at 500 °C (2 °C min^{-1})	ZnO/$ZnFe_2O_4$/C	100	100	1283	31
Zn–Co-BDC	Calcination in N_2 for 1 h at 400 °C (2 °C min^{-1}), then in air for 1 h at 600 °C (5 °C min^{-1})	Core/shell ZnO/$ZnCo_2O_4$/C	500	250	669	32
MIL-88B(Fe)	Calcination in Ar for 3 h at 600 °C	Fe_3O_4/C	462	200	928	33
MnO-doped MIL-53(Fe)	Annealing in Ar for 2 h 450 °C (2 °C min^{-1})	MnO/Fe_3O_4@C	200	200	1297	34
Fe_2Ni MIL-88	Annealing in H_2/Ar for 2 h at 500 °C, then annealing in air for 3 h at 300 °C	Hollow $NiFe_2O_4$ NSs@CNR	1830	1000	513	35
Fe_2Ni MIL-88	Annealing in air for 6 h at 450 °C (2 °C min^{-1})	Nanotubes $NiFe_2O_4/Fe_2O_3$	100	100	936	36
Ni-BDC	Calcination in air for hours at 550 °C (5 °C min^{-1})	Porous NiO	15	100	380	37
Mn-BDC	Thermal treatment to 250–300 °C	Mn_3O_4/C	700	120	592	38
Sn-BDC	Annealing in N_2 for 2 h at 500 °C (10 °C min^{-1})	SnO/C	50	100	950	39
Co-BTC	Calcination in air for 2 h at 550 °C (2 °C min^{-1})	Microfibers Co_3O_4	100	200	787	40
Co-BTC	Thermal treatment in air for 30 min at 500 °C (1 °C min^{-1})	Hierarchical Co_3O_4	100	90	529	41
[Cu_3(btc)$_2$]	Heated in N_2 for 30 min at 300 °C (10 °C min^{-1})	Hollow octahedra CuO	100	100	470	42
Cu-MOF-199	Pyrolyzed in air at 550 °C	CuO	100	40	484	43
Cu-BTC	Annealing in air for 10 h at 250 °C	Hollow nanorods CuO/C	100	200	505	44
Mn-BTC	Heating in N_2 for 2 h at 570 °C (10 °C min^{-1})	MnO/C	100	100	1221	45
Ni-BTC	Calcination in air at 500 °C for 2 h	Yolk–shell NiO	200	60	1060	46
Mn-BTC	Calcination for 3 h at 650 °C (2 °C min^{-1})	Porous nanobars Mn_2O_3	126	300	410	47
Zn-BTC/Ni	Annealing in Ar for 2 h at 450 °C (1 °C min^{-1})	Yolk–shell ZnO/$Ni_3ZnC_{0.7}$/C	500	750	1002	48
Mo/W/Cu-BTC	Annealing in N_2 for 6 h at 600 °C (2 °C min^{-1})	$Mo_xW_{1-x}O_2$–Cu@PC	500	250	911	49
Ni-BTC	Calcination in air for 1 h at 500 °C (2 °C min^{-1})	Mesoporous nanorods NiO	100	100	1019	50
ZIF-67	Calcination in N_2 for 30 min at 350 °C (5 °C min^{-1}) and 30 min in air	Dodecahedra Co_3O_4	100	100	780	51
Co-ZIF	Thermal treatment in Ar for 2 h at 300 °C	Film Co_3O_4	20 000	2000	300	52
ZIF-67/NGA	Calcination in air for 1 h at 300 °C (2 °C min^{-1})	Co_3O_4@NGN	1000	400	676	53
NCW@Fe-ZIFs	Calcination in Ar for 3 h at 500 °C (2 °C min^{-1})	Nanodots NCW@Fe_3O_4/NC	1000	600	1741	54
MIL-88B@ZIF-67	Calcination in air for 2 h at 500 °C (5 °C min^{-1})	Fe_2O_3@Co_3O_4	500	80	951	55
Ni–Co-ZIF-67	Calcination in air for 2 h at 400 °C (2 °C min^{-1})	$NiCo_2O_4$/NiO	200	100	1497	56
Zn–Fe-ZIF	Carbonization in N_2 for 2 h at 400 °C (2 °C min^{-1}), annealing in air for 2 h at 500 °C (10 °C min^{-1})	Hierarchical ZnO/$ZnFe_2O_4$/NC	200	100	1000	57
Zn–Co-ZIF/Ni	Annealing in N_2 for 3 h at 450 °C (3 °C min^{-1})	RGO/$ZnCo_2O_4$–ZnO–C/Ni	100	150	1184	58
Co–Mo-LDH@MXene	Annealing in N_2 for 2 h at 350 °C (0.5 °C min^{-1})	CoO/$Co_2Mo_3O_8$@MXene	2000	1200	545	59
PB	Three stages of annealing (below 350 °C, 550 °C, and 650 °C)	Hierarchical shell Fe_2O_3	200	200	950	60
3DG/PB	One-step annealing in air at 250 °C for 2 h	3DG/Fe_2O_3	5000	1200	523	61
Ni–Fe–PB	Calcination at 700 °C in air for 6 h (2 °C min^{-1})	$NiFe_2O_4$	1000	100	841	62
ZnFe–PB	Annealing in air for 3 h at 600 °C	ZnO/$ZnFe_2O_4$	1000	500	804	63
Fe–V–PB/PDA	Annealing to 500 °C at N_2 for 2 h (2 °C min^{-1})	Fe_3O_4/VO_x/C	500	400	742	64
PB/CeO_2	Calcination in air for 3 h at 400 °C (1 °C min^{-1})	Fe_3O_4/CeO_2	1000	3500	337	70

Transition metal oxides (TMOs) are a category of anode material candidates for LIBs owing to their larger theoretical capacity than that of the commercial graphite anode. By using 1,4-benzenedicarboxylic acid (H_2BDC) as an organic ligand, many MOF-derived TMOs, such as NiO,[18] SnO_2,[19] TiO_2,[20,21] and Fe_2O_3,[22,23] have been brought forward as promising anodes with high capacity and better cycling performance. Among various MOF-derived TMOs, Co_3O_4 is one of the most potential p-type semiconductor materials because of its high theoretical capacity (890 mA h g^{-1}), environmentally friendly nature and low cost. Bu *et al.* fabricated two-dimensional Co_3O_4 with wrinkled porous nanosheets by using a Co-based MOF (Co-BDC) as the template.[24] The resultant Co_3O_4 product exhibited an excellent capacity of 1477 mA h g^{-1} after 160 rounds. Even at the current rate up to 1 A g^{-1}, the capacity reached up to 775 mA h g^{-1} after 200 cycles. Hu *et al.* obtained mesoporous nanostructured Co_3O_4 based on a [Co(bdc)(DMF)] template by one-step calcination under air atmosphere. This Co_3O_4 anode material displayed a high discharge capacity of 913 mA h g^{-1} at 200 mA g^{-1} after 60 cycles.[25] The exceptional lithium storage performances were ascribed to the unique nanostructure, which shortened the transmission path of the Li ion and eased the volume change during repeated cycling. The initial charge and discharge capacities were 879.5 and 1286 mA h g^{-1}, respectively. The formation of SEI layers and interfacial lithium storage led to an irreversible capacity loss with a low coulombic efficiency of 68%.

Recently, many bimetallic MOFs have also been used as templates to fabricate bimetal oxides (M_xN_yO) with a spinel structure. Their electrochemical performances have been found to be superior to those of single metal oxides due to the synergic effect of the two active metals and the low activation energy of electron transportation. Kim *et al.* synthesized MOF-derived $Co_3V_2O_8$ with a sponge network, which offered an exceptional lithium storage capacity of 1000 mA h g^{-1} at 200 mA g^{-1}, and a good cycle performance of 501 mA h g^{-1} after 700 loops.[26] Interestingly, they also produced porous $Co_3V_2O_8$ microspheres by using a one-pot technique, which offered a specific discharge capacity of 940 mA h g^{-1} at 1 A g^{-1} after 100 rounds and 650 mA h g^{-1} at 5 A g^{-1} after 400 rounds.[27] The better rate performance was ascribed to the morphology and nanoscale dimensions of the electrode, which minimized the volume change during the lithiation and delithiation processes. The above-mentioned examples illustrated that the materials having the same composition but different morphologies may have different electrochemical properties.

Mixed transition-metal oxides (MTMOs) refer to chemical mixtures of metal oxides having two different metal cations, which should be distinguished from the physical mixture of two metal oxides. The MTMOs possess precise chemical composition and display better lithium storage capacity than single metal oxides due to their strong synergistic effect, enhanced ionic conductivity, electrochemical kinetics and mechanical stability. Xu *et al.* synthesized 3D hierarchical porous $ZnO/ZnCo_2O_4$ nanosheets by one-step thermal treatment, and the resultant products showed an outstanding reversible capacity of 1016 mA h g^{-1} at 5 A g^{-1}. A capacity of 630 mA h g^{-1} was maintained even at a high current rate of 10 A g^{-1}. To a certain extent, the mesopores and the porous space helped avoid the electrode pulverization problem and keep the electrode integrity intact.[28] Li *et al.* obtained yolk–shell ZnO/NiO microspheres by calcination treatment of bimetallic organic frameworks at 600 °C in air. This electrode delivered an excellent specific capacity of 1008.6 mA h g^{-1} after 200 rounds and a remarkable cycling stability of 592.4 mA h g^{-1} at 0.5 A g^{-1} after 1000 cycles. The unique yolk–shell structure can offer plenty of channels for electrolyte penetration and ionic transfer, which can also help compensate the volume changes of the anode during repeated cycling processes.[29]

In order to counter the issue of volume expansion and enhance the electrical conductivity of TMOs, an effective solution is to prepare TMO/C composites. One of the most important methods to obtain TMO/C composites is mixing/doping MOF-derived TMOs with *in situ* generation of porous carbon materials. Zou and co-workers used Fe(III)-modified MOF-5 as both the precursor and self-sacrificing template to fabricate new porous $ZnO/ZnFe_2O_4$/C octahedra with a hollow interior structure. When applied as an anode for LIBs, porous $ZnO/ZnFe_2O_4$/C octahedra showed better rate performance. Even at 10 A g^{-1}, the specific capacity reached up to 762 mA h g^{-1}, which is two-fold the theoretical capacity of graphite. The 3D carbon matrix is beneficial in hindering the volume changes during the lithiation and delithiation processes, which can ensure the structural integrity of the electrical circuit.[30] Chen *et al.* obtained hierarchical ball-in-ball $ZnO/ZnFe_2O_4$@C nanospheres through one-step carbonization. After the first 100 cycles at 100 mA g^{-1}, the reversible capacity of the products reached up to 1308 mA h g^{-1} due to the activation process of TMO-based electrodes during the cycling.[31] Moreover, Ge *et al.* obtained porous core–shell $ZnO/ZnCo_2O_4$/C hybrids by using ZnCo-MOF precursors as templates (Fig. 2). These electrodes displayed long-term and excellent cycling performance (the capacity can be retained at 669 mA h g^{-1} at 0.5 A g^{-1} after 250 loops), with average discharge capacities of 995, 953, 883, 844, and 715 mA h g^{-1} at current densities of 0.1, 0.2, 0.4, 0.8, and 1.6 A g^{-1}, respectively. The excellent electrochemical properties were ascribed to the coating of a carbon layer on the surface of $ZnCo_2O_4$ shells, which effectively enhanced the conductivity of the composite by preventing $ZnCo_2O_4$ from disintegration and aggregation. Moreover, the core–shell structure can provide enormous active sites and expand the contact area between the electrolyte and electrode.[32] Composites with carbon can improve the capacity of the active material to some extent. However, the existence of the C component in the TMO/C composite is significantly crucial. An excess of carbon will reduce the whole capacity of electrode materials since the C component cannot provide capacity as much as metal oxides can. Too low carbon content will limit the function of carbon contributing to the electron transfer. Therefore, it is of great significance to regulate the C content in TMO/C composites, which ensures improved electrical conductivity and meanwhile helps achieve the optimal specific capacity.[74,75]

In addition to the abovementioned MOF-derived metal oxides based on 1,4-benzenedicarboxylate, there is another class

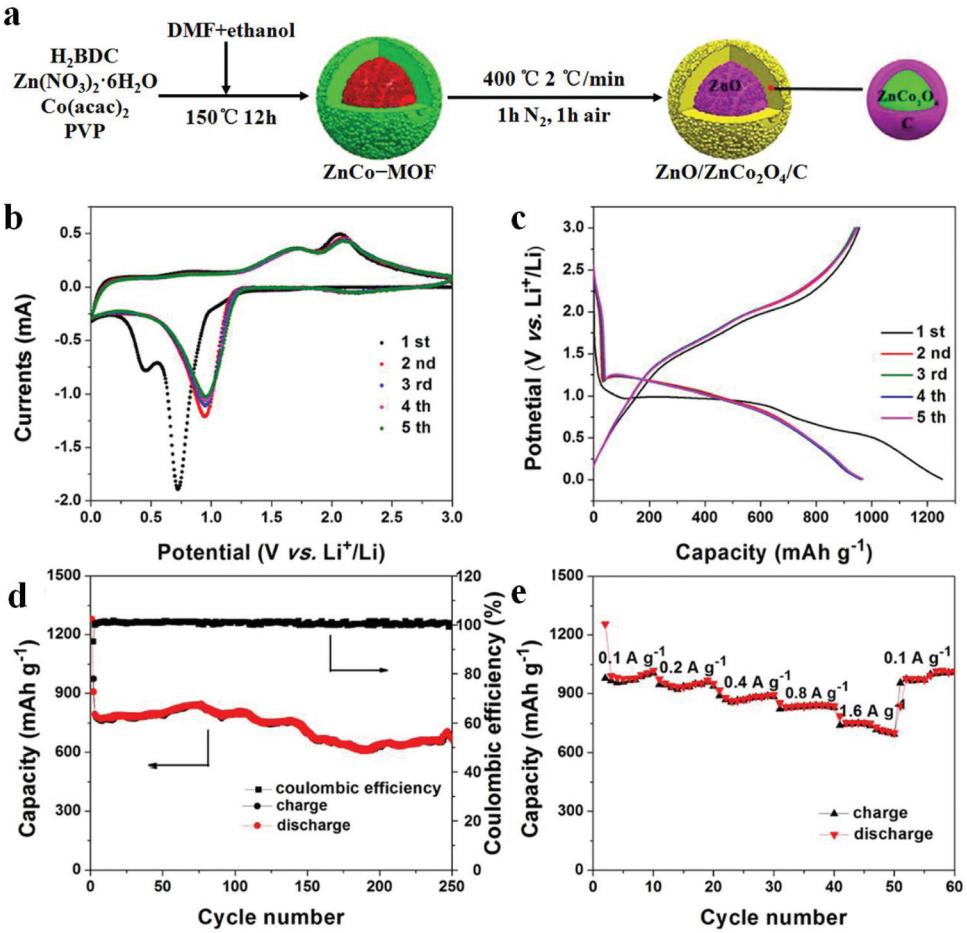

Fig. 2 (a) Preparation process of $ZnO/ZnCo_2O_4/C$ hybrids. (b) CV curves. (c) Charge/discharge profiles. (d) Cycling performance and coulombic efficiency. (e) Rate capability.[32]

of MOFs, named after Materials Institute Lavoisier, and is abbreviated as MILs. This kind of MOF is constructed from a 1,4-benzenedicarboxylate ligand and is suitable to synthesize iron oxides. For instance, Jin and co-workers obtained Fe_3O_4 and Fe_3O_4/C derived from MIL-88B through thermal treatment, and Fe_3O_4/C showed a high capacity of 928 mA h g^{-1} after 200 cycles.[33] Another example is MnO/Fe_3O_4@C nanospheres based on MIL-53 through one-step annealing under an Ar atmosphere.[34] The as-prepared electrode displayed a large capacity of 1297.5 mA h g^{-1} after 200 loops at 200 mA g^{-1}. The hierarchical porous microstructure was proved to be beneficial for the penetration of the electrolyte, shortening the movement path of Li^+ ions and boosting the ionic conductivity of the whole electrode system. The more effective electronic interaction between Fe_3O_4 and MnO species increased the electronic conductivity of the as-prepared nanospheres and also enhanced the reaction kinetics. Additionally, Gao *et al.* obtained $NiFe_2O_4$NSs@CNR and this anode delivered excellent electrochemical performance (an average capacity of 1355 mA h g^{-1} after 100 rounds).[35] In addition, Huang and co-workers synthesized Fe_2Ni MIL-88 nanorods *via* a hydrothermal method, which was used as a seed for the growth of a layer of Fe MIL-88 on the surface. Subsequently, the resulting core–shell Fe_2Ni MIL-88/Fe MIL-88 nanorods were heated at 450 °C for 6 h to generate hierarchical $NiFe_2O_4/Fe_2O_3$ nanotubes.[36] The electrode showed a good electrochemical performance of 936.9 mA h g^{-1} after 100 loops. The transmission electron microscopy (TEM) and high angle annular dark field scanning transmission electron microscopy (HAADF-STEM) images perfectly proved that the improved electrochemical behaviors originated from their hierarchical porous 1D structures, hollow tube structures, better redox chemistry and synergetic effect between nickel and iron ions (Fig. 3). The storage mechanisms involved in the electrochemical reaction during lithiation and delithiation are explained as follows:

$$NiFe_2O_4 + 8Li^+ + 8e^- \rightarrow Ni + 2Fe + 4Li_2O \quad (1)$$

$$Ni + Li_2O \leftrightarrow NiO + 2Li^+ + 2e^- \quad (2)$$

$$Fe_2O_3 + 6Li^+ + 8e^- \leftrightarrow 2Fe + 3Li_2O \quad (3)$$

2.2. TMOs derived from 1,3,5-benzenetricarboxylic acid based MOFs

In 1999, Williams and co-workers reported a new MOF called HKUST-1 ($[Cu_3(BTC)_2(H_2O)_3]_n$), which is synthesized with the

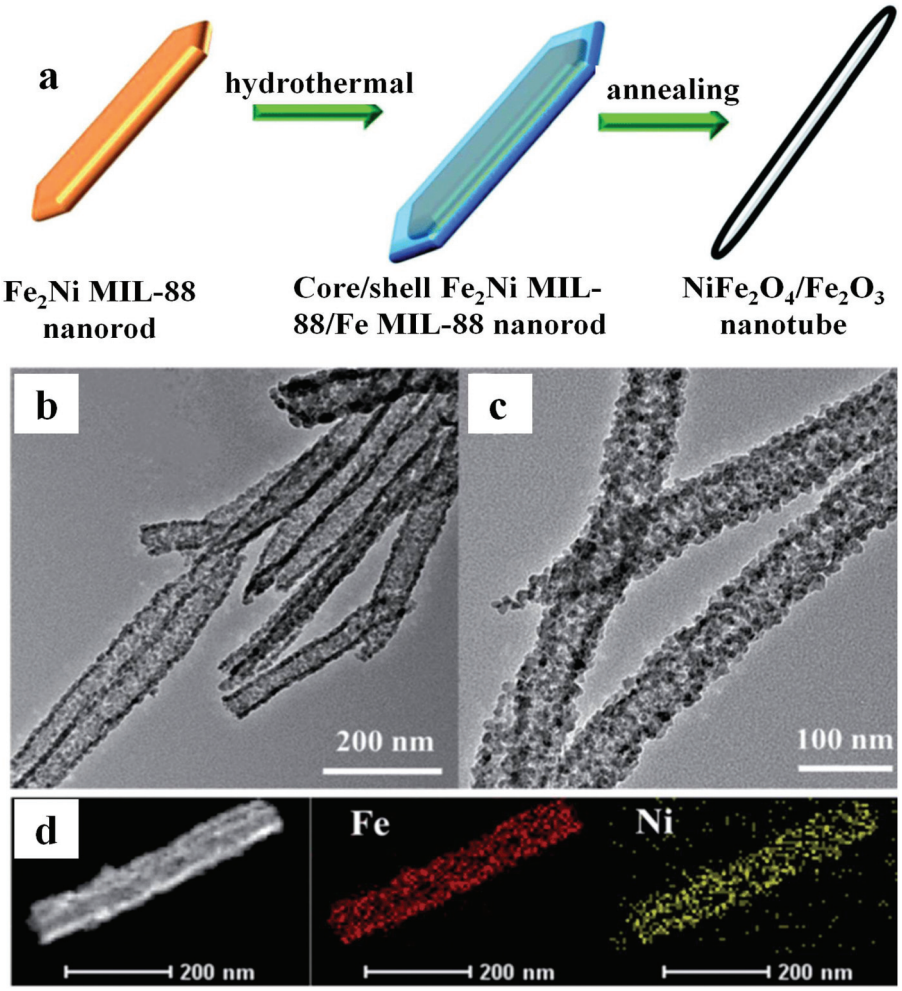

Fig. 3 (a) Preparation process of $NiFe_2O_4/Fe_2O_3$ nanotubes. (b) and (c) TEM images. (d) HAADF–STEM and elemental mapping.[36]

help of 1,3,5-benzenetricarboxylic acid as an organic moiety, whereas HKUST corresponds to Hong Kong University of Science and Technology.[76] This kind of MOF has a "pore–cage–pore" structure with open unsaturated Cu metal sites and presents excellent catalytic and adsorption properties.[77,78] 1,3,5-Benzenetricarboxylic acid (H_3BTC) is a rigid and planar molecule, in which the two carboxylate moieties are rigidly predisposed at 120°. As a good bridging ligand with oxygen donors, it has been extensively used for building multidimensional metal–organic networks. HKUST-1 is also known as MOF-199, which has been widely used as a template to synthesize suitable electrode materials due to its low price, easy preparation, high yield, and commercial availability.[43,79,80]

Recently, Chen *et al.* fabricated porous hollow Co_3O_4 microfibers *via* a chemical precipitation method, which demonstrated high lithium storage performance (1177.4 mA h g^{-1} under 100 mA g^{-1}) and long-term cycling capability (capacity of 787.6 mA h g^{-1} after 200 loops). The improved electrochemical performance was attributed to the large surface area (38.5 m^2 g^{-1}) and total pore volume (0.27 cm^3 g^{-1}), which offered large lithium storage sites and accelerated the movement speed of electrolyte molecules and Li^+ ions.[40] Zhang *et al.* obtained porous Co_3O_4 flower-like structures through a solvothermal method and subsequent thermal decomposition after 90 rounds under a current density of 100 mA g^{-1}, and the reversible capacity was still maintained at 529.2 mA h g^{-1}. It is worth noting that hierarchical porous Co_3O_4 structures displayed better electrochemical behavior due to their unique porous structures, which could perfectly compensate the volume expansion and facilitate lithium ion reactions during charge–discharge processes.[41]

Copper oxide (CuO) is another p-type semiconductor with great potential because of its improved safety, high theoretical capacity (674 mA h g^{-1}) and environmental benignity. Wu *et al.* synthesized porous CuO hollow octahedra by annealing of Cu-MOF templates. This as-prepared material delivered high reversible capacity and remarkable cycling stability, when assembled as an electrode. A capacity of 470 mA h g^{-1} was attained at 100 mA g^{-1} over 100 rounds. The good cyclability was ascribed to its porous octahedral morphology, hollow structure, and crystal plane structure, which was shown to have great influence on the electrochemical performance.[42]

Ogale and co-workers obtained CuO based on Cu-MOF-199 by controlled pyrolysis. This resultant CuO attained 90% of the initial reversible capacity after forty loops,[43] and even when the current rate reached up to 2 A g^{-1}, the capacity was still maintained at 210 mA h g^{-1}. Yin and his partners successfully prepared hollow porous CuO/C through controllable pyrolysis of $[Cu_3(btc)_2]_n$, and this electrode showed a good reversible capacity of 232.78 mA h g^{-1} at a high current rate of 3.2 A g^{-1}. The *in situ* generated amorphous carbon could improve the electrical conductivity. In addition, the hollow porous structure can mitigate the volume expansion/contraction and structure destruction problem, enhancing the cycling stability.[44]

In addition to the CuO and Co_3O_4 outlined above, many other TMOs have been fabricated, which showed distinctly enhanced electrochemical performances. For example, Zheng and colleagues developed ultrafine MnO nanocrystals incorporated within a porous carbon matrix. These MnO@C composites displayed an excellent capacity of 1221 mA h g^{-1} after 100 cycles.[45] Besides, Kong and co-authors have prepared yolk–shell NiO microspheres through a microwave-assisted hydrothermal method, which displayed a remarkable capacity of 1060 mA h g^{-1} at 0.2 A g^{-1} and good current performance (high capacity of 678, 612, and 454 mA h g^{-1} at 2, 3, and 5 A g^{-1}, respectively).[46] Maiti *et al.* obtained porous Mn_2O_3 nanobars by thermal treatment, where the resultant products showed an excellent cycling capability of 410 mA h g^{-1} over 300 cycles.[47]

Tremendous efforts have been put into the research on mixed transition metal oxides/carbon composite materials. Zhao *et al.* obtained yolk–shell $ZnO/Ni_3ZnC_{0.7}/C$ hybrid microspheres by using a solvothermal method (Fig. 4). This anode material showed outstanding cycling performance (high capacity of 1002 mA h g^{-1} over 750 loops) and rate capability.[48] The remarkable electrochemical behavior is mainly credited to the yolk–shell structure and tiny pore size, which offers large specific surface area and porosity, providing a large number of electrochemically active sites and more channels for the effective penetration of the electrolyte. Niu at al. obtained $Mo_{0.8}W_{0.2}O_2$–Cu@PC based on a polymetallic metal–organic framework (NENU-5) by thermal treatment at 600 °C under an atmosphere of an inert gas, and the ultra-long cycling performance and remarkable rate capability are mainly ascribed to the introduction of W and Cu elements.[49]

2.3. TMOs derived from 2-methylimidazole based MOFs

Zeolitic imidazolate frameworks (ZIFs) are a novel category of porous crystalline materials with the same topological structure as traditional zeolite molecular sieves.[81] ZIF compounds can be represented as $M(IM)_2$, where M and IM stand for metal ions and *N*-containing imidazole or imidazole derivative-based ligands, respectively. The angle of M–IM–M is similar to that of Si–O–Si (145°).[82] ZIFs not only displayed strong thermal stability and chemical stability, but also provided various structures and functions on adjusting the metal ions and organic linkers. This kind of MOF has been applied in gas storage and separation,[83] catalysis[84] and drug delivery[85] applications. However, ZIF-67 and ZIF-8 are two of the most typical representatives of ZIFs, which are linked by 2-methylimidazole anions with cobalt or zinc ions, respectively.[86] Metal oxide composites can be synthesized through post-modification of ZIF-67 or ZIF-8 and thermal treatment, which have huge application prospects as anode materials for LIBs.

Considering MOF-derived single metal oxides based on 2-methylimidazole, Wu *et al.* obtained porous hollow Co_3O_4 dodecahedra after the thermal treatment of an MOF at 350 °C. The porous hollow Co_3O_4 dodecahedra displayed a high

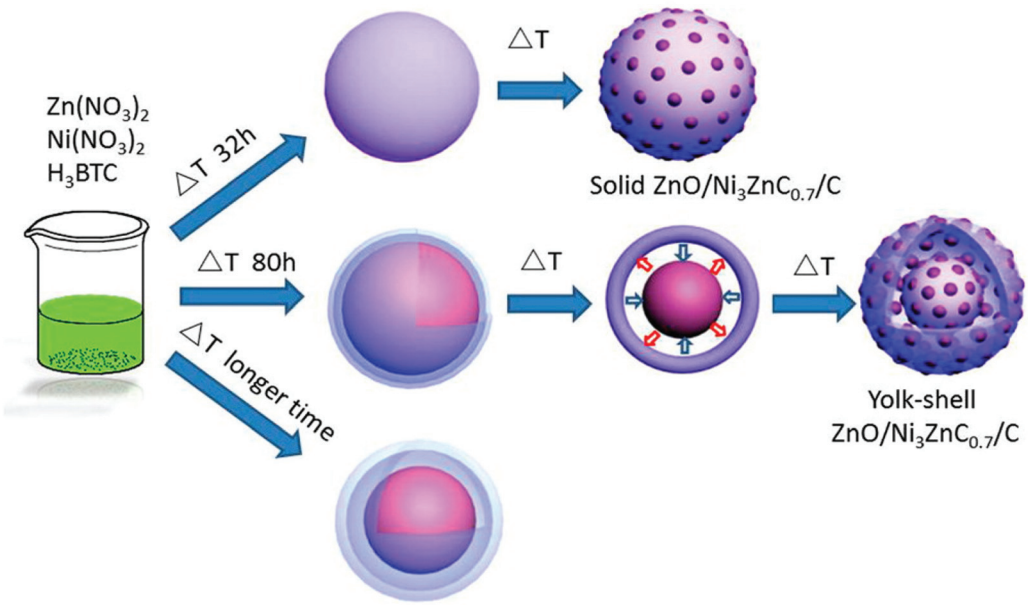

Fig. 4 Preparation process of yolk–shell $ZnO/Ni_3ZnC_{0.7}/C$.[48]

capacity of 780 mA h g^{-1} over 100 cycles.[51] Zhao and his partners reported a Co_3O_4 film with an electrochemically assisted process due to its good controllability and the *in situ* growth of MOFs during electrochemical processes.[52] These electrodes exhibited an impressive cycling performance of 2000 cycles at a current rate of 20 A g^{-1} and a coulombic efficiency of almost 100% after the 2000th cycle. In addition to mixing *in situ* porous carbon which retains the morphology of MOFs by high temperature carbonization with MOF-derived TMOs, the composite materials can be obtained by mixing/doping TMOs and external carbon sources (graphene oxide, carbon nanotubes, *etc.*). Sui *et al.* reported ZIF-67-derived porous Co_3O_4 in a N-doped graphene network (Co_3O_4/NGN) as the anode for LIBs. This as-prepared anode displayed high discharge capacity (955 mA h g^{-1} after 200 rounds), long-term cycling capability (676 mA h g^{-1} over 400 cycles), and remarkable rate performance. The existence of synergistic interactions between NGN and Co_3O_4 was credited for the good electrochemical performance. However, the initial decline in the discharge capacity was attributed to the formation of a solid electrolyte interphase (SEI) layer and an incomplete conversion reaction.[53]

Iron is a highly abundant metal in the Earth's crust, and because of that Fe_3O_4 has garnered much attention due to its low cost and a high theoretical capacity of 926 mA h g^{-1}. Wang *et al.* successfully synthesized ultrafine 3D hierarchical architecture Fe_3O_4 nanodots with N-doped carbon nanowebs (NCW@Fe_3O_4/NC). The initial cycle exhibits a discharge and charge capacity of 2867 and 1585 mA h g^{-1}, respectively, and a better coulombic efficiency (55.3%). The low initial low coulombic efficiency was ascribed to the irreversible lithium consumption of the NCW and Fe_3O_4 during the first cycle, while the conductive agent caused the irreversible capacity loss.[54]

Although single metal oxides and their carbon composites show good electrochemical behavior in lithium ion batteries, they still cannot fulfill the current demand in energy storage applications. Multi-component metal oxides have been developed for propelling the improvement of their electrochemical performance, such as ionic conductivity, electrochemical conductivity and mechanical stability. Zhang *et al.* obtained hierarchical Fe_2O_3@Co_3O_4 by using MIL-88B and ZIF-67 as an external iron source and an internal cobalt source, respectively.[55] This composite material displayed a high initial coulombic efficiency of 77% and a high capacity of 951 mA h g^{-1} at the end of 80 cycles. Sun and co-authors synthesized porous hollow $NiCo_2O_4$/NiO dodecahedra by using a solvothermal method.[56] This electrode demonstrated a high reversible capacity of 1535 mA h g^{-1} and excellent cycling behavior with 97.2% retention of coulombic efficiency over 100 loops.

The electrochemical behavior of multi-component metal oxides also can be enhanced through mixing/doping carbon, such as MOF-derived porous carbon, carbon nanotubes and MXenes. Ma *et al.* obtained ZnO/$ZnFe_2O_4$/N-doped C by calcining a ZnFe-MOF precursor and subsequently annealing the material in a muffle furnace for 2 hours under air atmosphere. This electrode displayed high specific capacity (after 100 loops at 200 mA g^{-1}, the capacity was retained at around 1000 mA h g^{-1}) and good cycling behavior. The unique structural features and N-doped carbon matrix offered extra conductivity for the electrode.[57] Li and co-authors synthesized an interesting sandwich-like $ZnCo_2O_4$–ZnO–C wrapped in reduced graphene oxide (RGO) on nickel foam. The RGO/$ZnCo_2O_4$–ZnO–C/Ni sandwich-like material showed the importance of RGO over the $ZnCo_2O_4$–ZnO–C/Ni anode without RGO. The RGO/$ZnCo_2O_4$–ZnO–C/Ni electrode exhibited a high capacity of 1184.4 mA h g^{-1} over 150 loops, whereas the capacity of $ZnCo_2O_4$–ZnO–C/Ni was 854.9 mA h g^{-1} under similar conditions. The RGO nanosheets serve as not only a conductive matrix, but also a flexible protector to anchor $ZnCo_2O_4$–ZnO–C on the Ni foam, in turn strengthening the mechanical stability of the anode during intercalation/de-intercalation processes.[58] Moreover, much attention has been paid to the usage of MXenes in lithium ion batteries due to their 2D structure, metallic conductivity, low diffusion barrier for lithium ions, and low volume changes during discharge–charge processes.[87] Zhao *et al.* successfully obtained a CoO/$Co_2Mo_3O_8$@MXene by annealing of a CoMO LDH polyhedron and an MXene at 350 °C under a N_2 atmosphere for 2 hours.[59] This mixed component metal oxide/MXene electrode showed better cycling behavior (the capacity was retained at 545 mA h g^{-1} at a current rate of 2 A g^{-1} at the end of 1200 cycles) and rate capability. It was demonstrated that the MXene played a significant role by efficiently reducing the charge–transfer impedance of CoO/$Co_2Mo_3O_8$ due to the decreased diameter of the semicircle at a high-frequency regime (Fig. 5).

2.4. TMOs derived from ferrocyanide based MOFs

Prussian Blue (PB) is one of the earliest artificial coordination compounds, which has been mostly used as a pigment and dye since its discovery. The open framework structure of PB is linked by transition metal ions and cyanide ligands, and it is composed of a mixed-valence iron(III) hexacyano ferrate(II) compound of $Fe_4[Fe(CN)_6]_3$ with a face-centered-cubic (fcc) crystal structure.[88–91] Generally, PB and Prussian blue analogues (PBAs) can be obtained from ferrocyanide ligands as starting resources, which can be converted into the corresponding metal oxides under controllable thermal treatment based on the Kirkendall effect and hold great potential applications as templates/precursors.[92–94]

Initially, Zhang *et al.* reported hierarchical shell-structured Fe_2O_3 microboxes based on $K_4Fe(CN)_6$, and compared the electrochemical performances of Fe_2O_3 obtained by heating treatment at different temperatures. It is worth noting that the decomposition of PB produced outward gas flow and led to the formation of an iron oxide shell with a large interior cavity. The as-prepared hierarchical shell-structured Fe_2O_3 microboxes displayed the highest capacity of 945 mA h g^{-1} at 200 mA g^{-1} over 30 rounds when compared to the other samples (Fe_2O_3 microboxes and porous Fe_2O_3 microboxes) under the same conditions.[60] Jiang *et al.* obtained porous Fe_2O_3 wrapping by 3D graphene (3DG) by one-step annealing of 3DG/PB at 250 °C in air. The as-prepared 3DG/Fe_2O_3 exhibi-

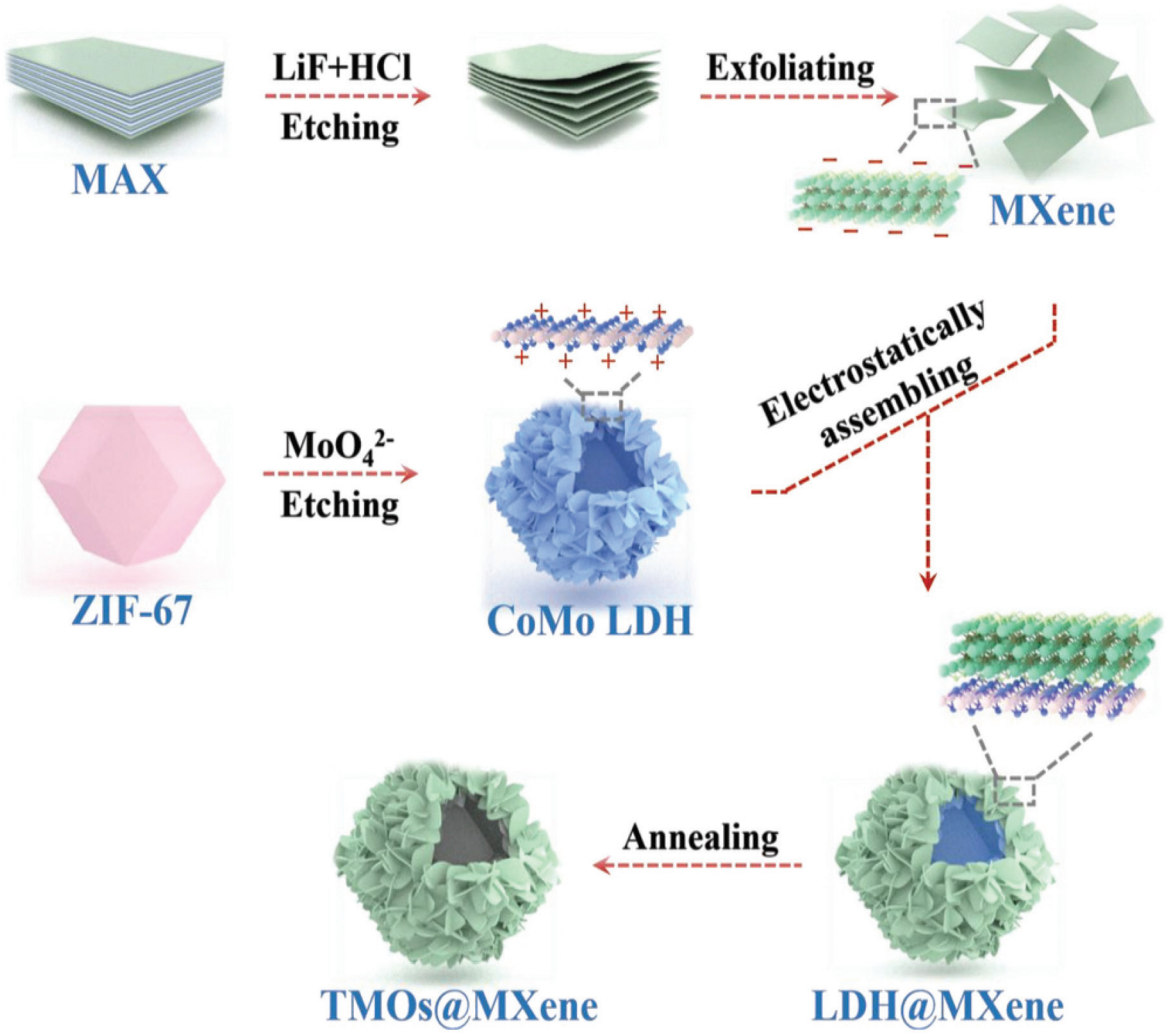

Fig. 5 Synthesis of $CoO/Co_2Mo_3O_8$@MXene hollow polyhedra.[59]

ted extraordinary cycling behavior (a high capacity of 523.5 mA h g^{-1} at a current rate of 5 A g^{-1} at the end of 1200 cycles) and good rate performance.[61]

In order to boost the electrochemical properties of PB-derived metal oxides, Yu *et al.* synthesized porous spinel AFe_2O_4 (A = Ni, Zn, Co) hollow structures. Among these, $NiFe_2O_4$ exhibited the most excellent electrochemical performance (high specific capacities of 841 and 447 mA h g^{-1} over 100 rounds at 1.0 and 5.0 A g^{-1}, respectively).[62] In addition, Yang *et al.* prepared a porous $ZnO/ZnFe_2O_4$ composite with a microwave-assisted synthesis protocol, where the as-prepared electrode showed excellent cycling stability (497 mA h g^{-1} after 1000 rounds at 2000 mA g^{-1}). Among them, ZnO can react with Fe_2O_3 to form $ZnFe_2O_4$ and it offers large specific capacity for the electrode.[63] Zhao *et al.* obtained carbon-coated Fe_3O_4/VO_x (Fe_3O_4/VO_x@C) hollow microboxes based on Prussian blue. The discharge capacity of Fe_3O_4/VO_x@C reached up to 742 mA h g^{-1} over 400 cycles. The electrochemical properties of Fe_3O_4/VO_x@C were proven to be better than those of Fe_3O_4 and Fe_3O_4@C, indicating the importance of the presence of VO_x in the as-prepared electrode.[64] Wang *et al.* mixed Ce $(NO_3)_2{\cdot}6H_2O$ and PB suspension, and then refluxed with stirring for 2 h. Subsequently, the resultant solid was heated at different temperatures for 3 h in air to produce Fe_2O_3@CeO_2 composites. The electrochemical performance of three electrodes (Fe_2O_3@CeO_2-400, Fe_2O_3@CeO_2-500, and Fe_2O_3@CeO_2-600) demonstrated the influence of calcination temperature on material properties (Fig. 6). Furthermore, CeO_2 was expected to play a significant role in this electrode by shortening the distance of lithium-ion diffusion, alleviating the volume expansion, and enhancing the thermal stability of the electrode. Furthermore, the CeO_2 layer can ease the collapse of Fe_2O_3 and enhance the electrode–electrolyte interface stability.[70]

2.5. TMOs derived from other unusual MOFs

As one brand of MOFs, porous coordination networks (PCNs) were developed and popularized by Zhou's group.[95] This kind of porous material contains multiple cubic octahedral nanopore cages and shows great potential in gas storage and adsorption.[96] However, probably due to the complicated syn-

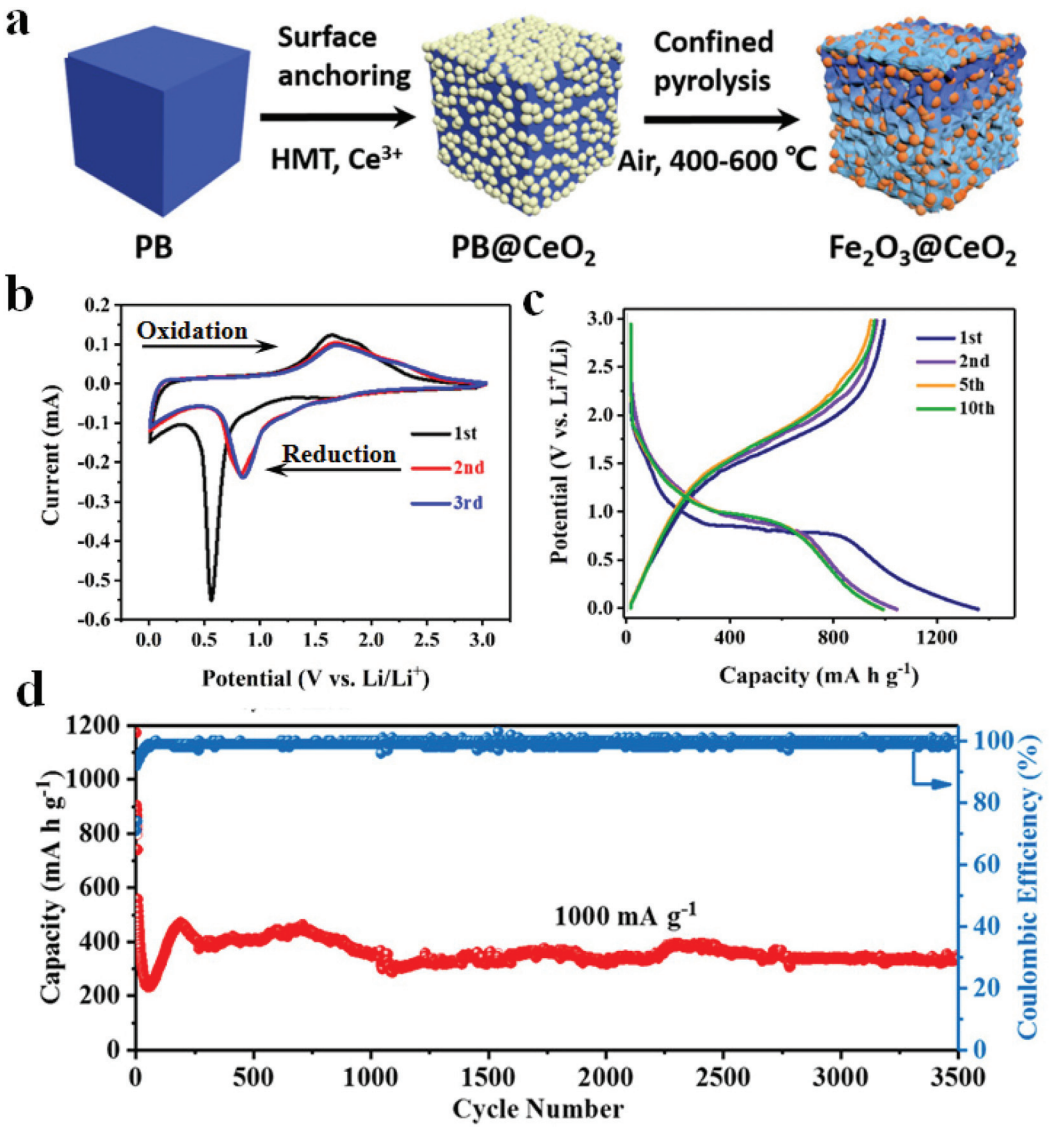

Fig. 6 (a) Schematic illustration of the Fe_2O_3@CeO_2 fabrication process. (b) CV curves of Fe_2O_3@CeO_2. (c) Voltage profiles at 100 mA g^{-1}. (d) Cycling performance.[70]

thetic methods of organic ligands and expensive raw materials, there are no examples of the application of metal oxides utilizing PCNs as precursors. In this section, we present some research results based on unusual organic linkers in order to broaden the discussion on the development of TMOs derived from various MOFs in the electrochemical energy storage and conversion field.

Hu and co-authors obtained manganese oxide (Mn_3O_4) from MOF-74 templates.[97] Hierarchical mesoporous MnO_x microcuboids possessed higher specific surface areas than Mn_2O_3 mesoporous nanobars, which exhibited most durable high rate performance and the highest capacity. Peng *et al.* synthesized a mesoporous spindle-like hollow CuO/C anode for LIBs based on $[Cu_2(abtc)(H_2O)_2]_3$ (H_4abtc = 1,1′-azobenzene-3,3,5,5-tetracarboxylic acid). This electrode delivered a high capacity of 789 mA h g^{-1} at the end of 200 cycles at 100 mA g^{-1}. When compared with other CuO hybrid anode materials, a better electrochemical performance of this anode was observed, which can be attributed to the advantages of structural and compositional features with hollow interior structure, small size, and porous characteristics.[98] Interestingly, by using another Mn-PBA MOF as a template constructed with 5-(4-pyridin-3-yl-benzoylamino)-isophthalic acid, mesoporous Mn_3O_4/C microspheres were obtained through thermolysis at 500 °C in air and they exhibited a large capacity of 1032 mA h g^{-1} over 500 rounds.[99] As it is well known that nitrogen-doping can substantially improve the electrochemical activity, N-rich organic ligands were usually chosen as precursors. For example, Kang and co-workers successfully obtained porous hollow Co_3O_4/N-doped carbon polyhedra based on $[Co_6O(TATB)_4](H_3O^+)_2$·Py (TATB = 2,4,6-tris(4-carboxyphenyl)-1,3,5-triazine and Py = pyridine) through a

solvothermal method (Fig. 7). The as-prepared porous anode displayed excellent electrochemical performance (620 mA h g^{-1} after 2000 rounds at 1000 mA g^{-1}). This electrode showed a capacity retention of 65% when the current density increased from 0.1 to 5.0 A g^{-1}.[100]

Much effort has also been put into the design of multi-metallic derivatives in order to improve the electrochemical behavior of LIBs. The multi-metallic materials can greatly utilize the advantages of different components and provide special performance through a reinforcement and/or modification between each metal.[101–103] Sun *et al.* obtained Fe–Mn–O/C microspheres based on Fe/Mn-MOF-74 (Fig. 8). This multi-metallic oxide displayed good cycle capability (1294 mA h g^{-1} over 200 cycles at 100 mA g^{-1}) and rate performance (722, 604,

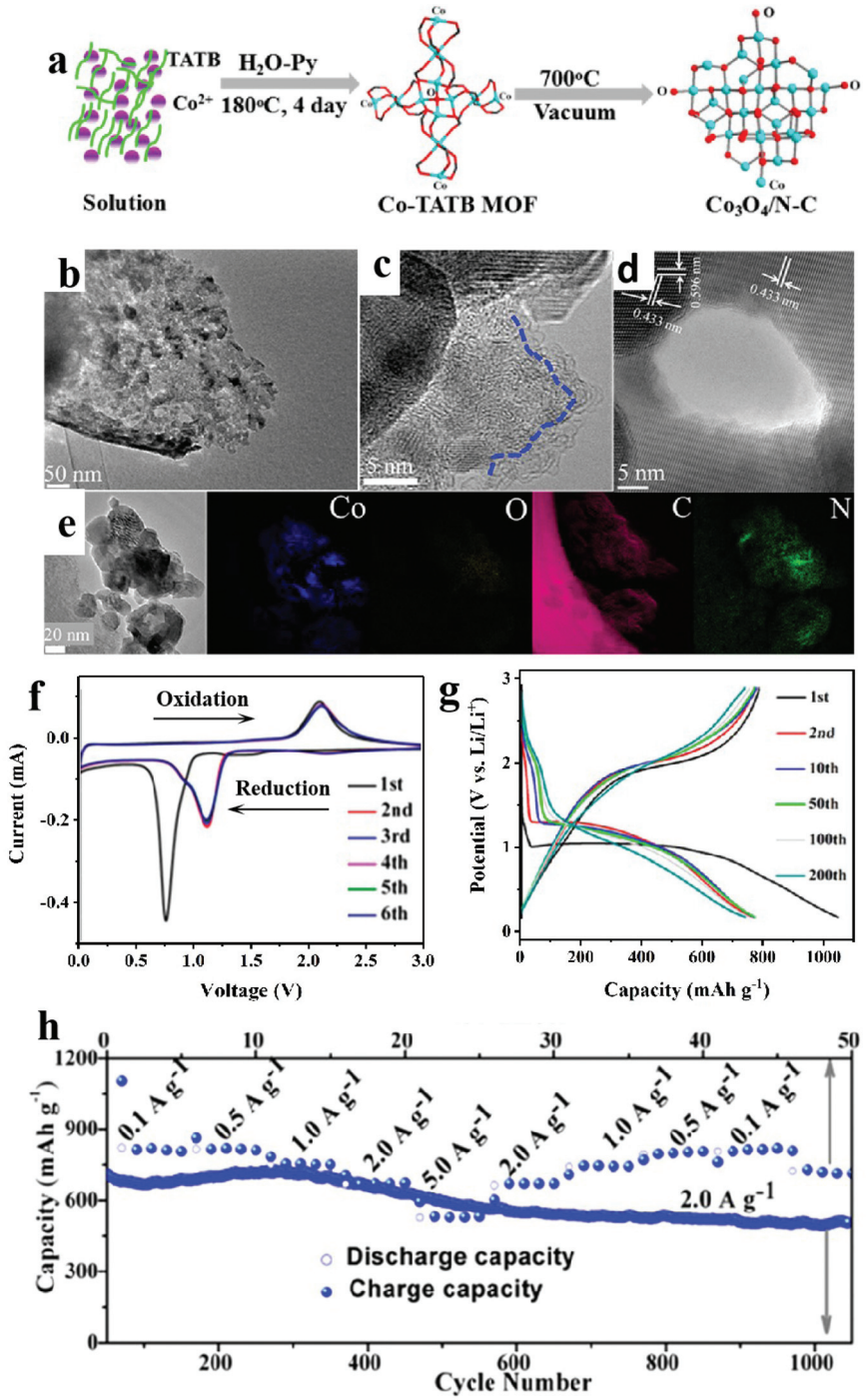

Fig. 7 (a) Schematic diagram of the fabrication processes of the Co_3O_4/N–C composite. (b) TEM images. (c and d) HRTEM images. (e) EELS elemental mapping images. (f) CV curves. (g) Charge–discharge profiles. (h) Rate capability.[98]

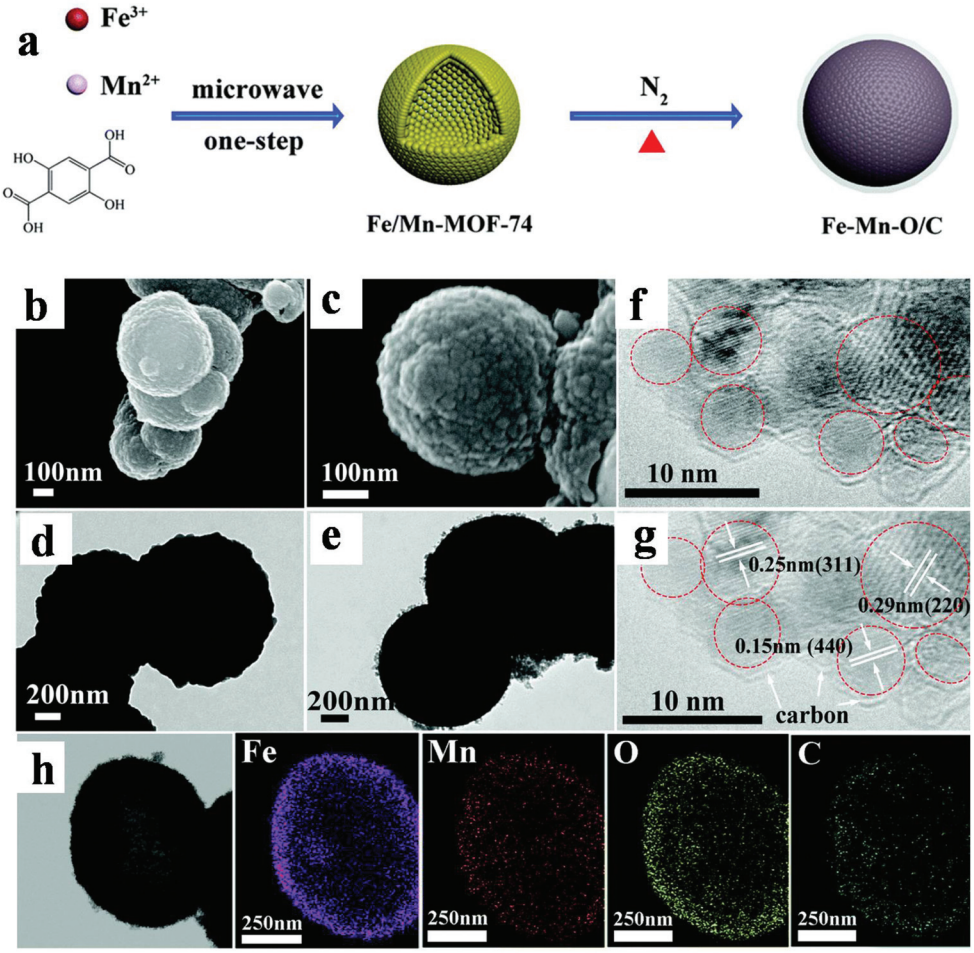

Fig. 8 (a) Schematic illustration of the synthesis of Fe/Mn-MOF-74 and Fe–Mn–O/C bimetal oxide. (b and c) SEM images. (d and e) TEM images. (f and g) HRTEM images. (h) Elemental mapping images.[104]

and 521 mA h g^{-1} at 0.2, 0.5, and 1 A g^{-1}, respectively). The remarkable electrochemical properties can be ascribed to the well-designed hollow microsphere morphology and synergistic effect between these two metal species.[104]

3. Summary and outlook

Great progress has been made in the field of lithium ion batteries (LIBs) over the past few decades as important energy storage devices. It has been established that the presence of a hollow/porous structure can exert a great influence on the electrochemical behavior of the anode. In order to address the abovementioned problems, much effort has been made in the development of MOF-derived metal oxides as anode materials for LIBs in green and facile ways. With the help of these strategies, various structures and morphologies of MOF-derived metal oxides and composites can be designed and prepared through annealing, microwave-assisted processes and solvothermal methods, eventually solving the problem of energy storage and conversion.

Although tremendous progress has been made in the application research of MOF-derived metal oxides, many issues still hinder the practical applications of these materials such as the following: (1) some organic linkers are too expensive and the synthetic routes are too complicated. Therefore, it is necessary to create simple, abundant, and green synthesis methods. (2) It is difficult to achieve mass production starting from MOF precursors to target materials due to the low-quality yield. Fortunately, some MOFs (ZIF-67, ZIF-8, MOF-5, *etc.*) are easily available from commercial resources, which provides us more confidence to study the detailed transformation pathway. In particular, different linkers for the use of these MOF-derived oxides for LIBs have significant effects on the morphology of the final product. For instance, MOF-5 and Prussian blue possess a cubic shape, while ZIF-8 or ZIF-67 presents a dodecahedral morphology. Following the previous comments and our practical perspective, 2-methylimidazole and ferricyanide should be better for serving as precursors to make metal oxides for LIBs in future studies. These two types of linkers contain abundant N elements, and the incorporation of optimized N-doping can lead to stronger binding with lithium

ions and enhance the electrochemical properties. Additionally, MOFs constructed with these two linkers can be generally used under mild conditions without heating or solvothermal reaction. This synthetic chemistry approach shows low energy consumption and is environmentally friendly. (3) Many TMOs derived from MOFs usually display low initial coulombic efficiency because of the side reactions originating from the decomposition of the electrolyte. However, effective strategies such as pre-lithiation techniques in surface chemistry can be put into practical applications. Nevertheless, MOF-derived metal oxides still hold the place of important potential templates in the electrochemical energy storage and conversion field due to their advantages of controllable structure, morphology and composition. Deeper insights into their working mechanisms can be achieved with the help of advanced instrumentation techniques. Overall, this review aims to provide information on interesting recent attempts and innovations by scientists and industrial partners who are planning to explore the application of TMOs as high-performance LIB anodes derived from MOFs.

Conflicts of interest

There are no conflicts to declare.

Acknowledgements

We gratefully acknowledge the financial support from Guangzhou Science and Technology Project, China (No. 201904010213).

Notes and references

1 P. Cai, K. Zou, G. Zou, H. Hou and X. Ji, Quinone/ester-based oxygen functional group-incorporated full carbon Li-ion capacitor for enhanced performance, *Nanoscale*, 2020, **12**, 3677–3685.
2 J. Chen, G. Zou, W. Deng, Z. Huang, X. Gao, C. Liu, S. Yin, H. Liu, X. Deng, Y. Tian, J. Li, C. Wang, D. Wang, H. Wu, L. Yang, H. Hou and X. Ji, Pseudo-bonding and electric-field harmony for Li-rich Mn-based oxide cathode, *Adv. Funct. Mater.*, 2020, 2004302.
3 C. Gao, Z. Jiang, P. Wang, L. R. Jensen, Y. Zhang and Y. Yue, Optimized assembling of MOF/SnO_2/graphene leads to superior anode for lithium ion batteries, *Nano Energy*, 2020, **74**, 104848.
4 J. M. Tarascon and M. Armand, Issues and challenges facing rechargeable lithium batteries, *Nature*, 2001, **414**, 359–367.
5 Y. Zhong, X. Xia and F. Shi, Transition metal carbides and nitrides in energy storage and conversion, *Adv. Sci.*, 2016, **3**, 1500286.
6 M. Mohamedali, H. Ibrahim and A. Henni, Incorporation of acetate-based ionic liquids into a zeolitic imidazolate framework (ZIF-8) as efficient sorbents for carbon dioxide capture, *Chem. Eng. J.*, 2018, **334**, 817–828.
7 H. Chen, K. Shen, Q. Mao, J. Chen and Y. Li, Nanoreactor of MOF-derived yolk–shell Co@C–N: precisely controllable structure and enhanced catalytic activity, *ACS Catal.*, 2018, **8**, 1417–1426.
8 H. Zheng, Y. Zhang, L. Liu, W. Wan, P. Guo, A. M. Nystrom and X. Zou, One-pot synthesis of metal–organic frameworks with encapsulated target molecules and their applications for controlled drug delivery, *J. Am. Chem. Soc.*, 2016, **138**, 962–968.
9 H. Lv, X. Zhang, F. Wang, G. Lv, T. Yu, M. Lv, J. Wang, Z. Yi and J. Hu, ZIF-67-assisted construction of hollow core/shell cactus-like MnNiCo trimetal electrodes and Co, N dual-doped carbon electrodes for high-performance hybrid supercapacitors, *J. Mater. Chem. A*, 2020, **8**, 14287–14298.
10 Y. Liu, Z. Wang, Y. Zhong, M. Tade, W. Zhou and Z. Shao, Molecular design of mesoporous $NiCo_2O_4$ and $NiCo_2S_4$ with sub-micrometer-polyhedron architectures for efficient pseudocapacitive energy storage, *Adv. Funct. Mater.*, 2017, **27**, 1701229.
11 Y. Liu, X. Xu, Z. Shao and S. P. Jiang, Metal–organic frameworks derived porous carbon, metal oxides and metal sulfides-based compounds for supercapacitors application, *Energy Storage Mater.*, 2020, **26**, 1–22.
12 X. Li, F. Cheng, S. Zhang and J. Chen, Shape-controlled synthesis and lithium–storage study of metal–organic frameworks Zn_4O(1,3,5-benzenetribenzoate)$_2$, *J. Power Sources*, 2006, **160**, 542–547.
13 Y. Zhao, Z. Song, X. Li, Q. Sun, N. Cheng, S. Lawes and X. Sun, Metal organic frameworks for energy storage and conversion, *Energy Storage Mater.*, 2016, **2**, 35–62.
14 Y. Xu, Q. Li, H. Xue and H. Pang, Metal–organic frameworks for direct electrochemical applications, *Coord. Chem. Rev.*, 2018, **376**, 292–318.
15 Z. Xie, W. Xu, X. Cui and Y. Wang, Recent progress in metal–organic frameworks and their derived nanostructures for energy and environmental applications, *ChemSusChem*, 2017, **10**, 1645–1663.
16 S. Fang, D. Bresser and S. Passerini, Transition metal oxide anodes for electrochemical energy storage in lithium- and sodium-ion batteries, *Adv. Energy Mater.*, 2019, **10**, 1902485.
17 F. Klein, B. Jache, A. Bhide and P. Adelhelm, Conversion reactions for sodium-ion batteries, *Phys. Chem. Chem. Phys.*, 2013, **15**, 15876–15887.
18 V. Soundharrajan, B. Sambandam, J. Song, S. Kim, J. Jo, P. T. Duong, S. Kim, V. Mathew and J. Kim, Metal organic framework-combustion: A one-pot strategy to NiO nanoparticles with excellent anode properties for lithium ion batteries, *J. Energy Chem.*, 2018, **27**, 300–305.
19 Z. Sun, C. Cao and W. Q. Han, A scalable formation of nano-SnO_2 anode derived from tin metal–organic frameworks for lithium-ion battery, *RSC Adv.*, 2015, **5**, 72825–72829.

20 Z. Wang, X. Li, H. Xu, Y. Yang, Y. Cui, H. Pan, Z. Wang, B. Chen and G. Qian, Porous anatase TiO_2 constructed from a metal–organic framework for advanced lithium-ion battery anodes, *J. Mater. Chem. A*, 2014, **2**, 12571–12575.

21 Z. Xiu, M. H. Alfaruqi, J. Gim, J. Song, S. Kim, T. V. Thi, P. T. Duong, J. P. Baboo, V. Mathew and J. Kim, Hierarchical porous anatase TiO_2 derived from a titanium metal–organic framework as a superior anode material for lithium ion batteries, *Chem. Commun.*, 2015, **51**, 12274–12277.

22 A. Banerjee, V. Aravindan, S. Bhatnagar, D. Mhamane, S. Madhavi and S. Ogale, Superior lithium storage properties of α-Fe_2O_3 nano-assembled spindles, *Nano Energy*, 2013, **2**, 890–896.

23 W. Guo, W. Sun, L. P. Lv, S. Kong and Y. Wang, Microwave-assisted morphology evolution of Fe-based metal–organic frameworks and their derived Fe_2O_3 nanostructures for Li-ion storage, *ACS Nano*, 2017, **11**, 4198–4205.

24 A. Li, M. Zhong, W. Shuang, C. Wang, J. Liu, Z. Chang and X. H. Bu, Facile synthesis of Co_3O_4 nanosheets from MOF nanoplates for high performance anodes of lithium-ion batteries, *Inorg. Chem. Front.*, 2018, **5**, 1602–1608.

25 C. Li, T. Chen, W. Xu, X. Lou, L. Pan, Q. Chen and B. Hu, Mesoporous nanostructured Co_3O_4 derived from MOF template: a high-performance anode material for lithium-ion batteries, *J. Mater. Chem. A*, 2015, **3**, 5585–5591.

26 V. Soundharrajan, B. Sambandam, J. Song, S. Kim, J. Jo, S. Kim, S. Lee, V. Mathew and J. Kim, $Co_3V_2O_8$ Sponge network morphology derived from metal–organic framework as an excellent lithium storage anode material, *ACS Appl. Mater. Interfaces*, 2016, **8**, 8546–8553.

27 B. Sambandam, V. Soundharrajan, V. Mathew, J. Song, S. Kim, J. Jo, D. P. Tung, S. Kim and J. Kim, Metal–organic framework–combustion: a new, cost-effective and one-pot technique to produce a porous $Co_3V_2O_8$ microsphere anode for high energy lithium ion batteries, *J. Mater. Chem. A*, 2016, **4**, 14605–14613.

28 X. Xu, K. Cao, Y. Wang and L. Jiao, 3D hierarchical porous ZnO/$ZnCo_2O_4$ nanosheets as high-rate anode material for lithium-ion batteries, *J. Mater. Chem. A*, 2016, **4**, 6042–6047.

29 J. Li, D. Yan, S. Hou, T. Lu, Y. Yao, D. H. Chua and L. Pan, Metal–organic frameworks derived yolk–shell ZnO/NiO microspheres as high-performance anode materials for lithium-ion batteries, *Chem. Eng. J.*, 2018, **335**, 579–589.

30 F. Zou, X. Hu, Z. Li, Q. Long, C. Hu, R. Zeng, Y. Jiang and Y. Huang, MOF-derived porous ZnO/$ZnFe_2O_4$/C octahedra with hollow interiors for high-rate lithium-ion batteries, *Adv. Mater.*, 2014, **26**, 6622–6628.

31 Y. Chen, J. Wu, W. Yang, Y. Fu, Z. R. Hou, S. Chen, L. Zhang, Y. Song and L. Wang, Zn/Fe-MOFs-derived hierarchical ball-in-ball ZnO/$ZnFe_2O_4$@carbon nanospheres with exceptional lithium storage performance, *J. Alloys Compd.*, 2016, **688**, 211–218.

32 X. Ge, Z. Li, C. Wang and L. Yin, Metal–organic frameworks derived porous core/shell structured ZnO/$ZnCo_2O_4$/C hybrids as anodes for high-performance lithium-ion battery, *ACS Appl. Mater. Interfaces*, 2015, **7**, 26633–26642.

33 Y. Jin, C. Zhao, Y. Lin, D. Wang, L. Chen and C. Shen, Fe-based metal–organic framework and its derivatives for reversible lithium storage, *J. Mater. Sci. Technol.*, 2017, **33**, 768–774.

34 Z. He, K. Wang, S. Zhu, L. Huang, M. Chen, J. Guo, S. Pei, H. Shao and J. Wang, MOF-derived hierarchical MnO-doped Fe_3O_4@C composite nanospheres with enhanced lithium storage, *ACS Appl. Mater. Interfaces*, 2018, **10**, 10974–10985.

35 X. Gao, J. Wang, D. Zhang, K. Nie, Y. Ma, J. Zhong and X. Sun, Hollow $NiFe_2O_4$ nanospheres on carbon nanorods as a highly efficient anode material for lithium ion batteries, *J. Mater. Chem. A*, 2017, **5**, 5007–5012.

36 G. Huang, F. Zhang, L. Zhang, X. Du, J. Wang and L. Wang, Hierarchical $NiFe_2O_4$/Fe_2O_3 nanotubes derived from metal organic frameworks for superior lithium ion battery anodes, *J. Mater. Chem. A*, 2014, **2**, 8048–8053.

37 F. Zhang, D. Jiang and X. Zhang, Porous NiO materials prepared by solid-state thermolysis of a Ni-MOF crystal for lithium-ion battery anode, *Nano-Struct. Nano-Objects*, 2016, **5**, 1–6.

38 B. Sambandam, V. Soundharrajan, J. Song, S. Kim, J. Jo, D. P. Tung, S. Kim, V. Mathew and J. Kim, Sponge network-shaped Mn_3O_4/C anode derived from a simple, one-pot metal organic framework-combustion technique for improved lithium ion storage, *Inorg. Chem. Front.*, 2016, **3**, 1609–1615.

39 Z. Bian, A. Li, R. He, H. Song, X. Chen, J. Zhou and Z. Ma, Metal–organic framework-templated porous SnO/C polyhedrons for high-performance lithium-ion batteries, *Electrochim. Acta*, 2018, **289**, 389–396.

40 Y. Chen, Y. Wang, H. Yang, H. Gan, X. Cai, X. Guo, B. Xu, M. Lu and A. Yuan, Facile synthesis of porous hollow Co_3O_4 microfibers derived-from metal–organic frameworks as an advanced anode for lithium ion batteries, *Ceramurgia Int.*, 2017, **43**, 9945–9950.

41 L. Zhang, B. Yan, J. Zhang, Y. Liu, A. Yuan and G. Yang, Design and self-assembly of metal–organic framework-derived porous Co_3O_4 hierarchical structures for lithium-ion batteries, *Ceramurgia Int.*, 2016, **42**, 5160–5170.

42 R. Wu, X. Qian, F. Yu, H. Liu, K. Zhou, J. Wei and Y. Huang, MOF-templated formation of porous CuO hollow octahedra for lithium-ion battery anode materials, *J. Mater. Chem. A*, 2013, **1**, 11126–11129.

43 A. Banerjee, U. Singh, V. Aravindan, M. Srinivasan and S. Ogale, Synthesis of CuO nanostructures from Cu-based metal organic framework (MOF-199) for application as anode for Li-ion batteries, *Nano Energy*, 2013, **2**, 1158–1163.

44 Y. Sun, P. Zhang, B. Wang, J. Wu, S. Ning, A. Xie and Y. Shen, Hollow porous CuO/C nanorods as a high-per-

formance anode for lithium ion batteries, *J. Alloys Compd.*, 2018, **750**, 77–84.

45 F. Zheng, G. Xia, Y. Yang and Q. Chen, MOF-derived ultrafine MnO nanocrystals embedded in a porous carbon matrix as high-performance anodes for lithium-ion batteries, *Nanoscale*, 2015, **7**, 9637–9645.

46 S. Kong, R. Dai, H. Li, W. Sun and Y. Wang, Microwave hydrothermal synthesis of Ni-based metal–organic frameworks and their derived yolk–shell NiO for Li-ion storage and supported ammonia borane for hydrogen desorption, *ACS Sustainable Chem. Eng.*, 2015, **3**, 1830–1838.

47 S. Maiti, A. Pramanik and S. Mahanty, Electrochemical energy storage in Mn_2O_3 porous nanobars derived from morphology-conserved transformation of benzenetricarboxylate-bridged metal–organic framework, *CrystEngComm*, 2016, **18**, 450–461.

48 Y. Zhao, X. Li, J. Liu and C. Wang, MOF-derived ZnO/$Ni_3ZnC_{0.7}$/C hybrids yolk–shell microspheres with excellent electrochemical performances for lithium ion batteries, *ACS Appl. Mater. Interfaces*, 2016, **8**, 6472–6480.

49 S. Niu, Z. Wang, T. Zhou, M. Yu, M. Yu and J. Qiu, A polymetallic metal–organic framework-derived strategy toward synergistically multidoped metal oxide electrodes with ultralong cycle life and high volumetric capacity, *Adv. Funct. Mater.*, 2017, **27**, 1605332.

50 H. Pang, B. Guan, W. Sun and Y. Wang, Metal–organic-frameworks derivation of mesoporous NiO nanorod for high-performance lithium ion batteries, *Electrochim. Acta*, 2016, **213**, 351–357.

51 R. Wu, X. Qian, X. Rui, H. Liu, B. Yadian, K. Zhou, J. Wei, Q. Yan, X. Q. Feng and Y. Long, Zeolitic imidazolate framework 67-derived high symmetric porous Co_3O_4 hollow dodecahedra with highly enhanced lithium storage capability, *Small*, 2014, **10**, 1932–1938.

52 G. Zhao, X. Sun, L. Zhang, X. Chen, Y. Mao and K. Sun, A self-supported metal–organic framework derived Co_3O_4 film prepared by an in-situ electrochemically assistant process as Li ion battery anodes, *J. Power Sources*, 2018, **389**, 8–12.

53 Z. Y. Sui, P. Y. Zhang, M. Y. Xu, Y. W. Liu, Z. X. Wei and B. H. Han, Metal–organic framework-derived metal oxide embedded in nitrogen-doped graphene network for high-performance lithium-ion batteries, *ACS Appl. Mater. Interfaces*, 2017, **9**, 43171–43178.

54 Y. Wang, Y. Gao, J. Shao, R. Holze, Z. Chen, Y. Yun, Q. Qu and H. Zheng, Ultrasmall Fe_3O_4 nanodots within N-doped carbon frameworks from MOFs uniformly anchored on carbon nanowebs for boosting Li-ion storage, *J. Mater. Chem. A*, 2018, **6**, 3659–3666.

55 S. L. Zhang, B. Y. Guan and H. B. Wu, Metal–organic framework-assisted synthesis of compact Fe_2O_3 nanotubes in Co_3O_4 host with enhanced lithium storage properties, *Nano-Micro Lett.*, 2018, **10**, 44.

56 C. Sun, J. Yang, X. Rui, W. Zhang, Q. Yan, P. Chen, F. Huo, W. Huang and X. Dong, MOF-directed templating synthesis of a porous multicomponent dodecahedron with hollow interiors for enhanced lithium-ion battery anodes, *J. Mater. Chem. A*, 2015, **3**, 8483–8488.

57 Y. Ma, Y. Ma, D. Geiger, U. Kaiser, H. Zhang, G. T. Kim, T. Diemant, R. J. Behm, A. Varzi and S. Passerini, ZnO/$ZnFe_2O_4$/N-doped C micro-polyhedrons with hierarchical hollow structure as high-performance anodes for lithium-ion batteries, *Nano Energy*, 2017, **42**, 341–352.

58 Z. Li and L. Yin, Sandwich-like reduced graphene oxide wrapped MOF-derived $ZnCo_2O_4$-ZnO-C on nickel foam as anodes for high performance lithium ion batteries, *J. Mater. Chem. A*, 2015, **3**, 21569–21577.

59 X. Zhao, H. Xu, Z. Hui, Y. Sun, C. Yu, J. Xue, R. Zhou, L. Wang, H. Dai and Y. Zhao, Electrostatically assembling 2D nanosheets of MXene and MOF-derivatives into 3D hollow frameworks for enhanced lithium storage, *Small*, 2019, **15**, 1904255.

60 L. Zhang, H. B. Wu, S. Madhavi, H. H. Hng and X. W. Lou, Formation of Fe_2O_3 microboxes with hierarchical shell structures from metal–organic frameworks and their lithium storage properties, *J. Am. Chem. Soc.*, 2012, **134**, 17388–17391.

61 T. Jiang, F. Bu, X. Feng, I. Shakir, G. Hao and Y. Xu, Porous Fe_2O_3 nanoframeworks encapsulated within three-dimensional graphene as high-performance flexible anode for lithium-ion battery, *ACS Nano*, 2017, **11**, 5140–5147.

62 H. Yu, H. Fan, B. Yadian, H. Tan, W. Liu, H. H. Hng, Y. Huang and Q. Yan, General approach for MOF-derived porous spinel AFe_2O_4 hollow structures and their superior lithium storage properties, *ACS Appl. Mater. Interfaces*, 2015, **7**, 26751–26757.

63 X. Yang, H. Xue, Q. Yang, R. Yuan, W. Kang and C. S. Lee, Preparation of porous ZnO/$ZnFe_2O_4$ composite from metal organic frameworks and its applications for lithium ion batteries, *Chem. Eng. J.*, 2017, **308**, 340–346.

64 Z. W. Zhao, T. Wen, K. Liang, Y. F. Jiang, X. Zhou, C. C. Shen and A. W. Xu, Carbon-coated Fe_3O_4/VO_x hollow microboxes derived from metal–organic frameworks as a high-performance anode material for lithium-ion batteries, *ACS Appl. Mater. Interfaces*, 2017, **9**, 3757–3765.

65 K. Wang, C. Wu, F. Wang, N. Jing and G. Jiang, Co/Co_3O_4 nanoparticles coupled with hollow nanoporous carbon polyhedrons for the enhanced electrochemical sensing of acetaminophen, *ACS Sustainable Chem. Eng.*, 2019, **7**, 18582–18592.

66 D. T. Lee, J. Zhao, C. J. Oldham, G. W. Peterson and G. N. Parsons, UiO-66-NH_2 metal–organic framework (MOF) nucleation on TiO_2, ZnO, and Al_2O_3 atomic layer deposition-treated polymer fibers: role of metal oxide on MOF growth and catalytic hydrolysis of chemical warfare agent simulants, *ACS Appl. Mater. Interfaces*, 2017, **9**, 44847–44855.

67 G. Li, H. Cai, X. Li, J. Zhang, D. Zhang, Y. Yang and J. Xiong, Construction of hierarchical $NiCo_2O_4$@Ni-MOF hybrid arrays on carbon cloth as superior battery-type

electrodes for flexible solid-state hybrid supercapacitors, *ACS Appl. Mater. Interfaces*, 2019, **11**, 37675–37684.

68 H. Gao, Y. Luan, K. Chaikittikul, W. Dong, J. Li, X. Zhang, D. Jia, M. Yang and G. Wang, A facile in situ self-assembly strategy for large-scale fabrication of CHS@MOF yolk/shell structure and its catalytic application in a flow system, *ACS Appl. Mater. Interfaces*, 2015, **7**, 4667–4674.

69 K. M. Choi, H. M. Jeong, J. H. Park, Y. B. Zhang, J. K. Kang and O. M. Yaghi, Supercapacitors of nanocrystalline metal–organic frameworks, *ACS Nano*, 2014, **8**, 7451–7457.

70 K. Wang, F. Zhang, G. Zhu, H. Zhang, Y. Zhao, L. She and J. Yang, Surface anchoring approach for growth of CeO_2 nanocrystals on Prussian blue capsules enable superior lithium storage, *ACS Appl. Mater. Interfaces*, 2019, **11**, 33082–33090.

71 O. M. Yaghi and H. Li, Hydrothermal synthesis of a metal–organic framework containing large rectangular channels, *J. Am. Chem. Soc.*, 1995, **117**, 10401–10402.

72 O. M. Yaghi, G. M. Li and H. Li, Selective binding and removal of guests in a microporous metal–organic framework, *Nature*, 1995, **738**, 703–706.

73 N. L. Rosi, J. Eckert, M. Eddaoudi, D. T. Vodak, J. Kim, M. O'Keeffe and O. M. Yaghi, Hydrogen storage in microporous metal–organic frameworks, *Science*, 2003, **300**, 1127–1130.

74 K. Li, F. Shua, X. Guo and D. Xue, High performance porous MnO@C composite anode materials for lithium-ion batteries, *Electrochim. Acta*, 2016, **188**, 793–800.

75 R. Jiao, L. Zhao, S. Zhou, Y. Zhai, D. Wei, S. Zeng and X. Zhang, Effects of carbon content and current density on the Li^+ storage performance for MnO@C nanocomposite derived from Mn-based complexes, *Nanomaterials*, 2020, **10**, 1629.

76 S. S.-Y. Chui, S. M.-F. Lo, J. P. H. Charmant, A. G. Orpen and I. D. Williams, A chemically functionalizable nanoporous material $[Cu_3(TMA)_2(H_2O)_3]_n$, *Science*, 1999, **283**, 1148–1150.

77 M. I. Mohideen, B. Xiao, P. S. Wheatley, A. C. McKinlay, Y. Li, A. M. Slawin, D. W. Aldous, N. F. Cessford, T. Duren, X. Zhao, R. Gill, K. M. Thomas, J. M. Griffin, S. E. Ashbrook and R. E. Morris, Protecting group and switchable pore-discriminating adsorption properties of a hydrophilic–hydrophobic metal–organic framework, *Nat. Chem.*, 2011, **3**, 304–310.

78 C. Y. L. Sun, X. S. Liang, D. Dong, K. Z. Shao;, Y. H. Ren and Z. M. Su, Highly stable crystalline catalysts based on a microporous metal–organic framework and polyoxometalates, *J. Am. Chem. Soc.*, 2009, **131**, 1883–1888.

79 E. A. Jafari, M. Moradi, S. Borhani, H. Bigdeli and S. Hajati, Fabrication of hybrid supercapacitor based on rod-like HKUST-1@polyaniline as cathode and reduced graphene oxide as anode, *Phys. E*, 2018, **99**, 16–23.

80 D. D. Zu, L. Lu, X. Q. Liu, D. Y. Zhang and L. B. Sun, Improving hydrothermal stability and catalytic activity of metal–organic frameworks by graphite oxide incorporation, *J. Phys. Chem. C*, 2014, **118**, 19910–19917.

81 B. Wang, A. P. Cote, H. Furukawa, M. O'Keeffe and O. M. Yaghi, Colossal cages in zeolitic imidazolate frameworks as selective carbon dioxide reservoirs, *Nature*, 2008, **453**, 207–211.

82 A. Phan, C. J. Doonan, F. J. Uribe-Romo, C. B. Knobler, M. O'Keeffe and O. M. Yaghi, Synthesis, structure, and carbon dioxide capture properties of zeolitic imidazolate frameworks, *Acc. Chem. Res.*, 2010, **43**, 58–67.

83 R. Banerjee, A. Phan, B. Wang, C. Knobler, H. Furukawa, M. O'Keeffe and O. M. Yaghi, High-throughput synthesis of zeolitic imidazolate frameworks and application to CO_2 capture, *Science*, 2008, **319**, 939–943.

84 H. L. Jiang, B. Liu, T. Akita, M. Haruta, H. Sakurai and Q. Xu, Au@ZIF-8: CO oxidation over gold nanoparticles deposited to metal–organic framework, *J. Am. Chem. Soc.*, 2009, **131**, 11302–11303.

85 J. Zhuang, C. H. Kuo, L. Y. Chou, D. Y. Liu, E. Weerapana and C. K. Tsung, Optimized metal–organic-framework nanospheres for drug delivery: Evaluation of small-molecule encapsulation, *ACS Nano*, 2014, **8**, 2812–2819.

86 D. Matatagui, A. Sainz-Vidal, I. Gràcia, E. Figueras, C. Cane and J. M. Saniger, Chemoresistive gas sensor based on ZIF-8/ZIF-67 nanocrystals, *Sens. Actuators, B*, 2018, **274**, 601–608.

87 G. Zou, B. Ge, H. Zhang, Q. Zhang, C. Fernandez, W. Li, J. Huang and Q. Peng, Self-reductive synthesis of MXene/$Na_{0.55}Mn_{1.4}Ti_{0.6}O_4$ hybrids for high-performance symmetric lithium ion batteries, *J. Mater. Chem. A*, 2019, **7**, 7516–7525.

88 M. Hu, S. Furukawa, R. Ohtani, H. Sukegawa, Y. Nemoto, J. Reboul, S. Kitagawa and Y. Yamauchi, Synthesis of Prussian blue nanoparticles with a hollow interior by controlled chemical etching, *Angew. Chem., Int. Ed.*, 2012, **51**, 984–988.

89 S. Vaucher, M. Li and S. Mann, Synthesis of prussian blue nanoparticles and nanocrystal superlattices in reverse microemulsions, *Angew. Chem., Int. Ed.*, 2000, **112**, 1793–1796.

90 X. Shen, S. Wu, Y. Liu, K. Wang, Z. Xu and W. Liu, Morphology syntheses and properties of well-defined prussian blue nanocrystals by a facile solution approach, *J. Colloid Interface Sci.*, 2009, **329**, 188–195.

91 X. L. Wu, M. Cao, C. Hu and X. He, Sonochemical synthesis of prussian blue nanocubes from a single-source precursor, *Cryst. Growth Des.*, 2006, **6**, 26–28.

92 Y. Guo, G. Qin, E. Liang, M. Li and C. Wang, MOFs-derived $MgFe_2O_4$ microboxes as anode material for lithium-ion batteries with superior performance, *Ceram. Int.*, 2017, **43**, 12519–12525.

93 L. Hou, L. Lian, L. Zhang, G. Pang, C. Yuan and X. Zhang, Self-sacrifice template fabrication of hierarchical mesoporous bi-component-active ZnO/$ZnFe_2O_4$ sub-microcubes as superior anode towards high-performance lithium-ion battery, *Adv. Funct. Mater.*, 2015, **25**, 238–246.

94 F. Zheng, D. Zhu, X. Shi and Q. Chen, Metal–organic framework-derived porous $Mn_{1.8}Fe_{1.2}O_4$ nanocubes with an interconnected channel structure as high-performance anodes for lithium ion batteries, *J. Mater. Chem. A*, 2015, **3**, 2815–2824.

95 M. Bosch, S. Yuan, W. Rutledge and H. C. Zhou, Stepwise synthesis of metal–organic frameworks, *Acc. Chem. Res.*, 2017, **50**, 857–865.

96 D. Zhao, D. J. Timmons, D. Yuan and H. C. Zhou, Tuning the topology and functionality of metal–organic frameworks by ligand design, *Acc. Chem. Res.*, 2011, **44**, 123–133.

97 X. Hu, X. Lou, C. Li, Q. Yang, Q. Chen and B. Hu, Green and rational design of 3D layer-by-layer MnO_x hierarchically mesoporous microcuboids from MOF templates for high-rate and long-life Li-ion batteries, *ACS Appl. Mater. Interfaces*, 2018, **10**, 14684–14697.

98 H. J. Peng, G. X. Hao, Z. H. Chu, C. L. He, X. M. Lin and Y. P. Cai, Mesoporous spindle-like hollow CuO/C fabricated from a Cu-based metal–organic framework as anodes for high-performance lithium storage, *J. Alloys Compd.*, 2017, **727**, 1020–1026.

99 H. J. Peng, G. X. Hao, Z. H. Chu, J. Lin, X. M. Lin and Y. P. Cai, Mesoporous Mn_3O_4/C microspheres fabricated from MOF template as advanced lithium-ion battery anode, *Cryst. Growth Des.*, 2017, **17**, 5881–5886.

100 W. Kang, Y. Zhang, L. Fan, L. Zhang, F. Dai, R. Wang and D. Sun, Metal–organic framework derived porous hollow Co_3O_4/N–C polyhedron composite with excellent energy storage capability, *ACS Appl. Mater. Interfaces*, 2017, **9**, 10602–10609.

101 M. Huang, K. Mi, J. Zhang, H. Liu, T. Yu, A. Yuan, Q. Kong and S. Xiong, MOF-derived bi-metal embedded N-doped carbon polyhedral nanocages with enhanced lithium storage, *J. Mater. Chem. A*, 2017, **5**, 266–274.

102 H. Li, M. Liang, W. Sun and Y. Wang, Bimetal–organic framework: One-step homogenous formation and its derived mesoporous ternary metal oxide nanorod for high-capacity, high-rate, and long-cycle-life lithium storage, *Adv. Funct. Mater.*, 2016, **26**, 1098–1103.

103 H. Li, Y. Su, W. Sun and Y. Wang, Carbon nanotubes rooted in porous ternary metal sulfide@N/S-doped carbon dodecahedron: Bimetal–organic-frameworks derivation and electrochemical application for high-capacity and long-life lithium-ion batteries, *Adv. Funct. Mater.*, 2016, **26**, 8345–8353.

104 W. Sun, S. Chen and Y. Wang, A metal–organic-framework approach to engineer hollow bimetal oxide microspheres towards enhanced electrochemical performances of lithium storage, *Dalton Trans.*, 2019, **48**, 2019–2027.